1 Supplementary material for PAPER-2021-038

This appendix contains supplementary material to the measurements. Eq. 1 gives the the $B^0 \to K^0_S e^+ e^-$and $B^+ \to K^{*+} e^+ e^-$differential branching fractions divided by the branching fractions of their respective normalisation modes. Fig. 1 shows the total efficiencies for the four signal decay modes as function of q^2. Figs. 2 and 3 show differential measurements of $r^{-1}_{J/\psi K^{(*)}}$. Figs. 4 and 5 show the profile likelihood scans for $R^{-1}_{K^{(*)}}$ and the differential branching fractions. Fig. 6 compares the measurements of $R^{-1}_{K^{(*)}}$ presented in this Letter with previous measurements by the Belle collaboration. Fig. 7 shows the $J/\psi K^{(*)}$ invariant mass spectra and the maximum likelihood fits use to determine the $B \to J/\psi K^{(*)}$control mode yields with a linear scale. Figs. 8 and 9 show the $\psi(2S)K^{(*)}$ invariant mass spectra and the maximum likelihood fits use to determine the $B \to \psi(2S)K^{(*)}$ mode yields with linear and logarithmic scales.

In the main text, the differential branching fractions of $B^0 \to K^0_S e^+ e^-$and $B^+ \to K^{*+} e^+ e^-$decays are reported. These are normalised using the world-average branching fractions for $B^0 \to J/\psi\,(e^+e^-)\,K^0$ and $B^+ \to J/\psi\,(e^+e^-)\,K^{*+}$ respectively [1]. The ratios of signal and control mode branching fractions used in this calculation are

$$\begin{aligned}
&\frac{\mathrm{d}\mathcal{B}\left(B^0 \to K^0 e^+ e^-\right)}{\mathrm{d}q^2} \Big/ \mathcal{B}\left(B^0 \to J/\psi\left(e^+e^-\right)K^0\right) = \\
&\qquad \left(4.9\,^{+1.2}_{-1.1}\,(\text{stat.}) \pm 0.2\,(\text{syst.})\right) \times 10^{-4}\ \text{GeV}^{-2}c^4, \\
&\frac{\mathrm{d}\mathcal{B}\left(B^+ \to K^{*+} e^+ e^-\right)}{\mathrm{d}q^2} \Big/ \mathcal{B}\left(B^+ \to J/\psi\left(e^+e^-\right)K^{*+}\right) = \\
&\qquad \left(1.08\,^{+0.22}_{-0.21}\,(\text{stat.})\,^{+0.06}_{-0.04}\,(\text{syst.})\right) \times 10^{-3}\ \text{GeV}^{-2}c^4, \qquad (1)
\end{aligned}$$

where $B^+ \to K^{*+} e^+ e^-$candidates are selected with $m(K^0_S\pi^+)$ within 300 MeV/c^2 of the world-average K^{*+} mass, whereas $B^+ \to J/\psi\,(e^+e^-)\,K^{*+}$candidates are selected in the range $792 < m(K^0_S\pi^+)/\,\text{MeV}/c^2 < 992$.

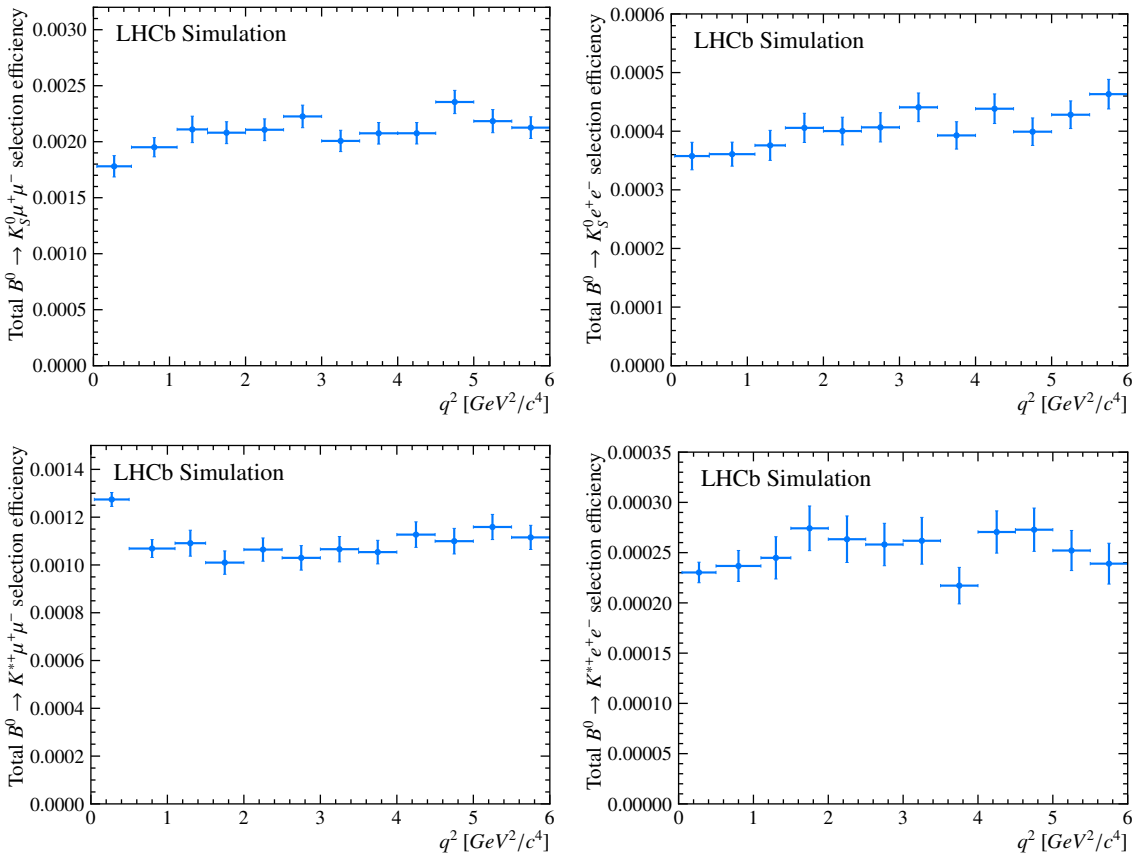

Figure 1: Total selection efficiencies as a function of q^2, for (top left) $B^0 \to K^0_S \mu^+ \mu^-$, (top right) $B^0 \to K^0_S e^+ e^-$, (bottom left) $B^+ \to K^{*+} \mu^+ \mu^-$, and (bottom right) $B^+ \to K^{*+} e^+ e^-$ decays. The efficiencies are evaluated using simulated candidates that have been corrected to improve agreement with data. These efficiencies account for detector resolution effects including the effect of bremsstrahlung, which may cause a candidate to be reconstructed in a different bin of q^2 than would be dictated by its 'true' value.

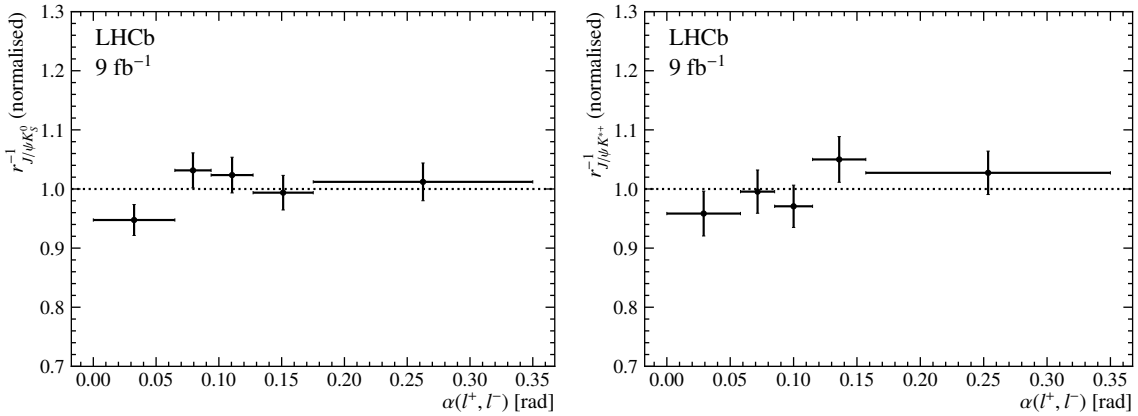

Figure 2: Single ratios (left) $r^{-1}_{J/\psi K^0_S}$ and (right) $r^{-1}_{J/\psi K^{*+}}$ as a function of the opening angle of the two leptons, normalised to their average value.

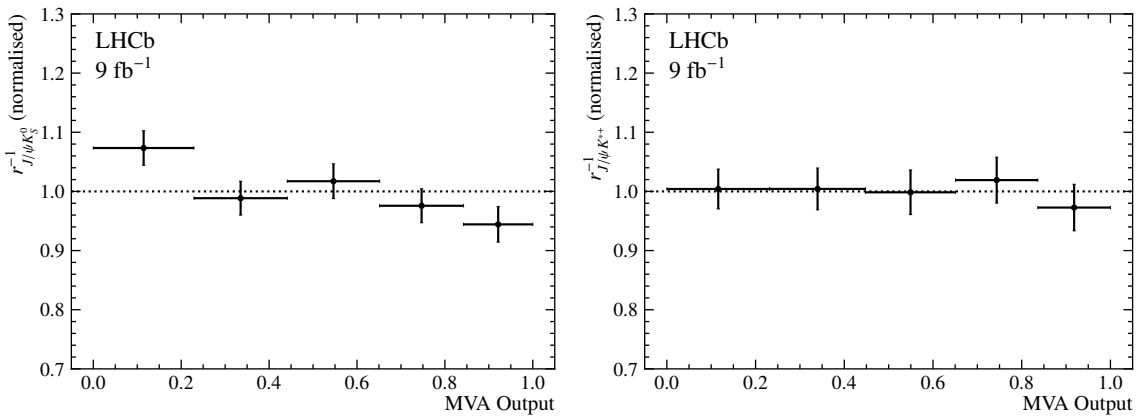

Figure 3: Single ratios (left) $r^{-1}_{J/\psi K^0_S}$ and (right) $r^{-1}_{J/\psi K^{*+}}$ as a function of the output of an MVA trained to separate the signal and control modes, normalised to their average value.

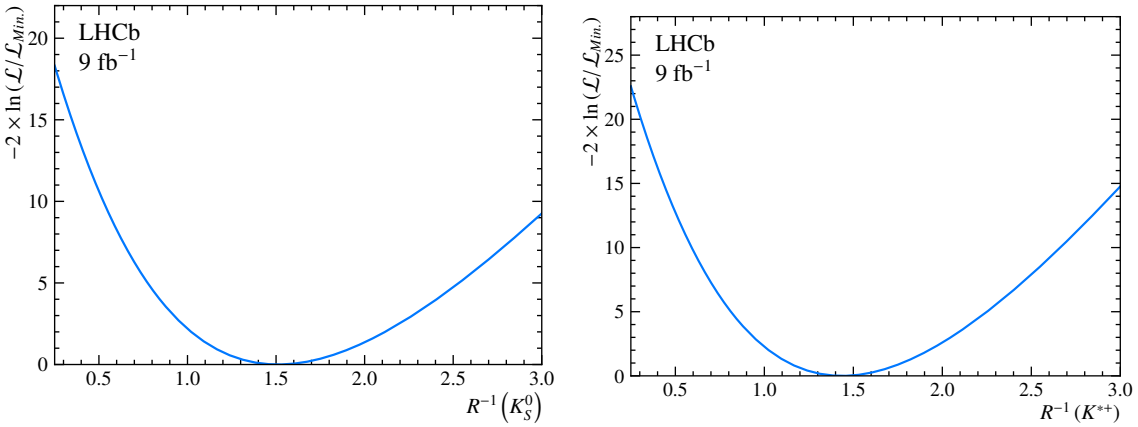

Figure 4: Scans of the profile likelihoods as a function of (left) $R^{-1}_{K^0_S}$, and (right) $R^{-1}_{K^{*+}}$.

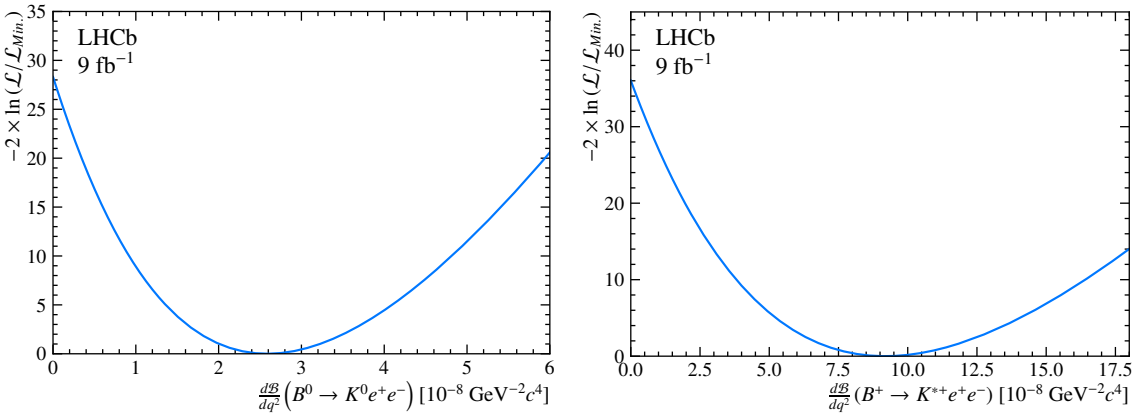

Figure 5: Scans of the profile likelihoods as a function of the differential branching fractions for (left) $B^0\to K^0e^+e^-$ decays, and (right) $B^+\to K^{*+}e^+e^-$ decays.

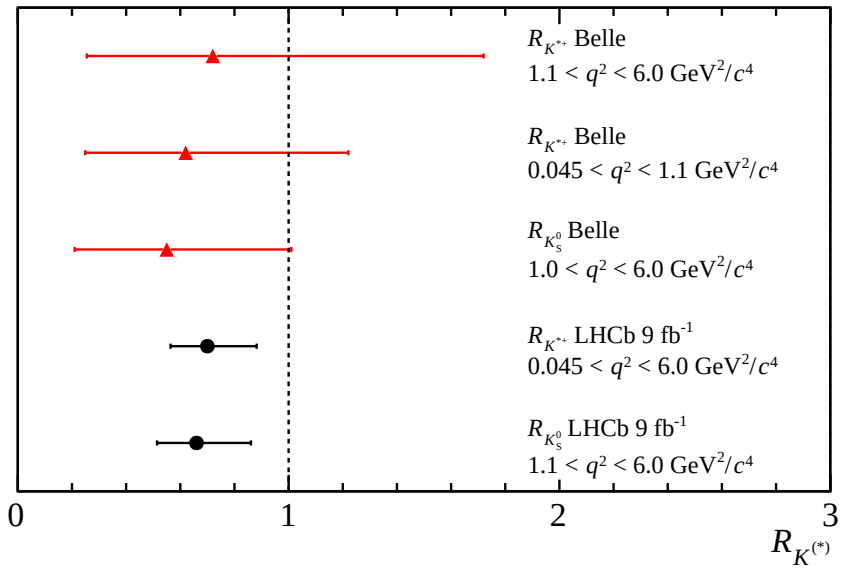

Figure 6: Measurements of $R_{K^0_S}$ and $R_{K^{*+}}$ performed by the LHCb and Belle collaborations [2,3].

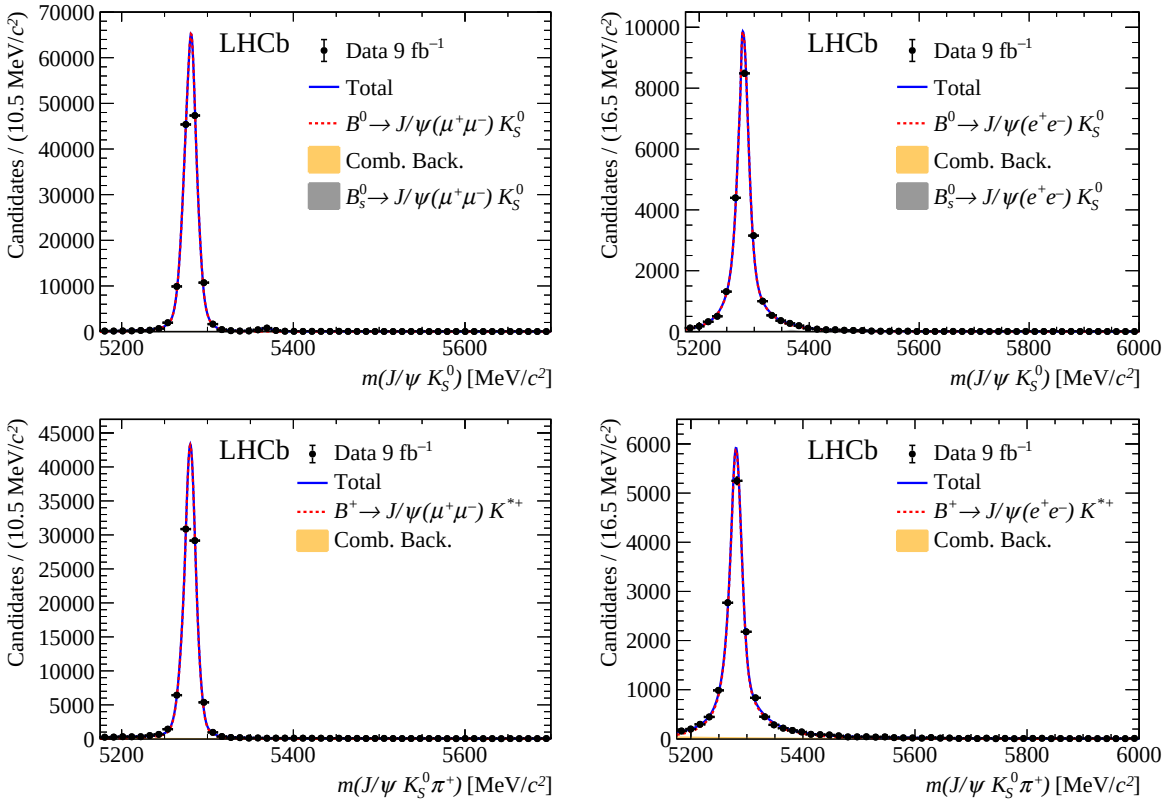

Figure 7: Distributions of (top left) $J/\psi(\mu^+\mu^-)K^0_S$ mass, (top right) $J/\psi(e^+e^-)K^0_S$ mass, (bottom left) $J/\psi(\mu^+\mu^-)K^0_S\pi^+$ mass and (bottom right) $J/\psi(e^+e^-)K^0_S\pi^+$ mass with the fit models used to determine the control mode yields.

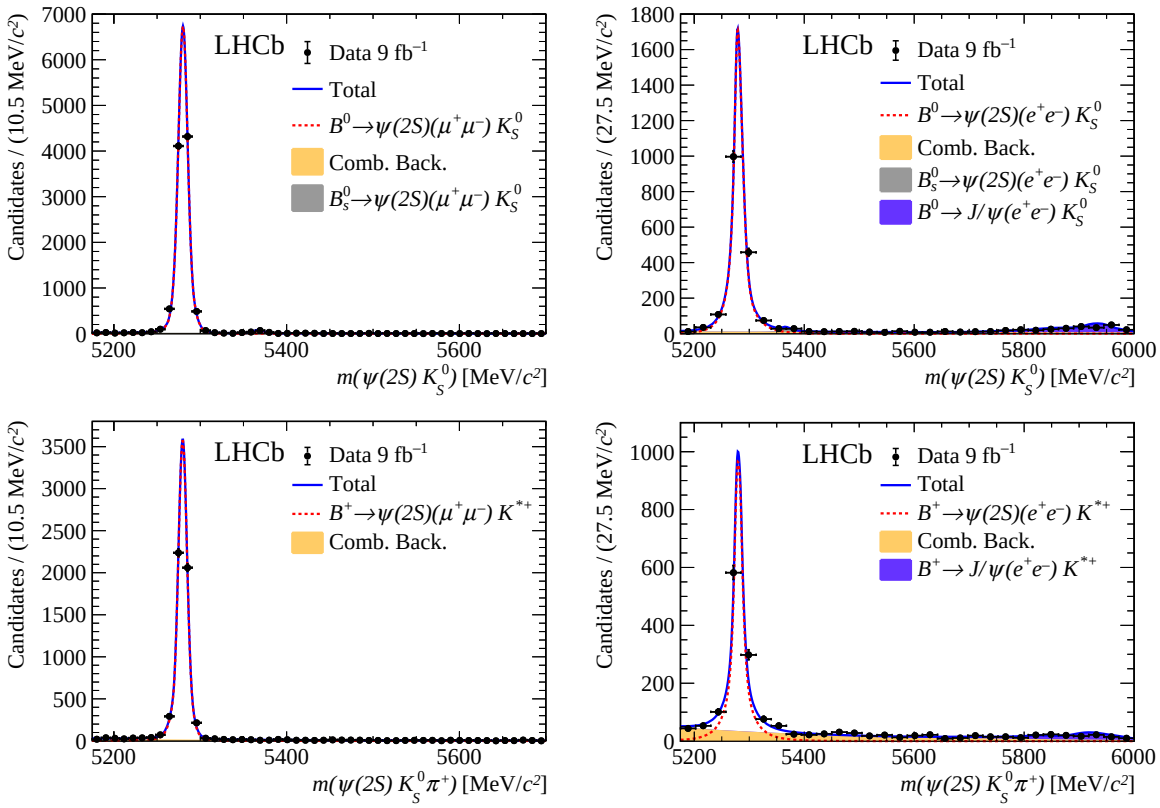

Figure 8: Distributions of (top left) $\psi(2S)(\mu^+\mu^-)K^0_S$ mass, (top right) $\psi(2S)(e^+e^-)K^0_S$ mass, (bottom left) $\psi(2S)(\mu^+\mu^-)K^0_S\pi^+$ mass and (bottom right) $\psi(2S)(e^+e^-)K^0_S\pi^+$ mass with the fit models used to determine the $\psi(2S)$ control mode yields.

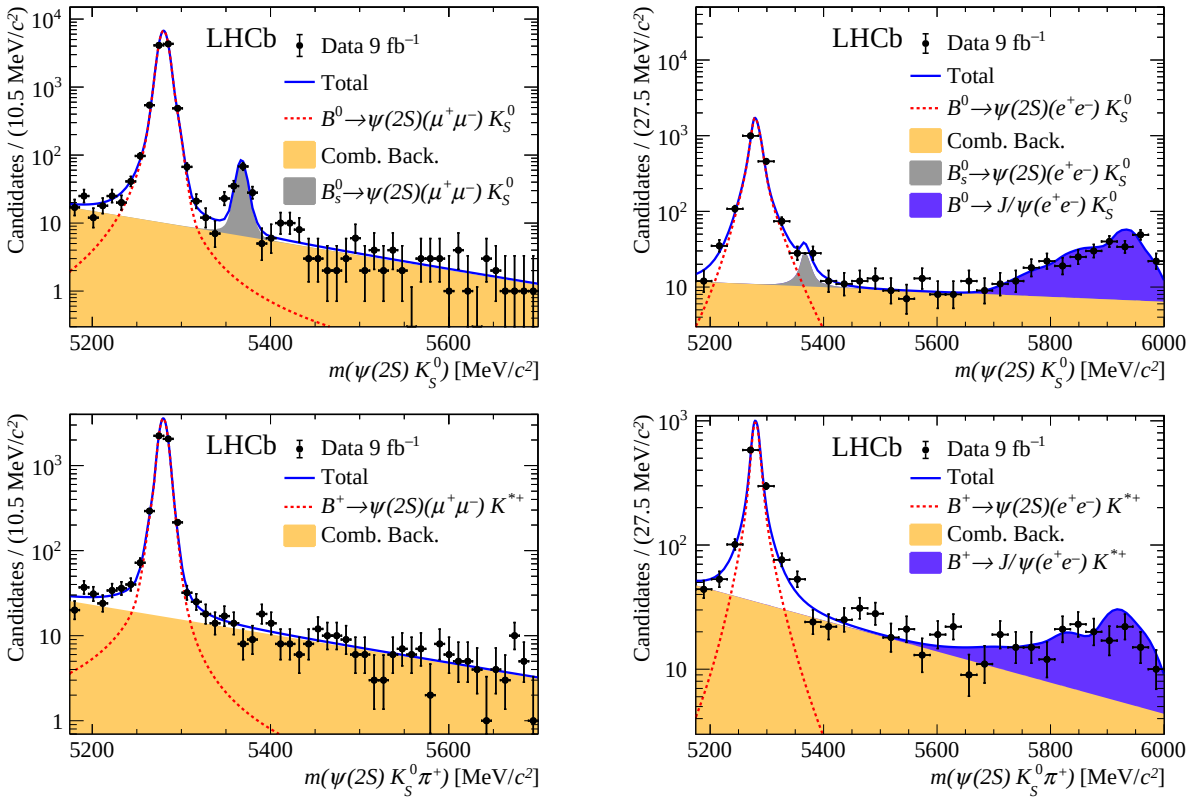

Figure 9: Distributions of (top left) $\psi(2S)(\mu^+\mu^-)K^0_S$ mass, (top right) $\psi(2S)(e^+e^-)K^0_S$ mass, (bottom left) $\psi(2S)(\mu^+\mu^-)K^0_S\pi^+$ mass and (bottom right) $\psi(2S)(e^+e^-)K^0_S\pi^+$ mass with the fit models used to determine the $\psi(2S)$ control mode yields.

References

[1] Particle Data Group, P. A. Zyla *et al.*, *Review of particle physics*, Prog. Theor. Exp. Phys. **2020** (2020) 083C01.

[2] Belle collaboration, A. Abdesselam *et al.*, *Test of lepton-flavor universality in $B \to K^* \ell^+ \ell^-$ decays at Belle*, Phys. Rev. Lett. **126** (2021) 161801, arXiv:1904.02440.

[3] Belle collaboration, S. Choudhury *et al.*, *Test of lepton flavor universality and search for lepton flavor violation in $B \to K \ell\ell$ decays*, JHEP **03** (2021) 105, arXiv:1908.01848.